Eur. Phys. J. B **7**, 331–335 (1999)

THE EUROPEAN PHYSICAL JOURNAL B

EDP Sciences

Multi-anticipative car-following model

H. Lenz[a], C.K. Wagner, and R. Sollacher

Siemens AG, Corporate Technology, Information and Communications, ZT IK 4, Otto-Hahn-Ring 6, 81730 Munich, Germany

Received: 23 March 1998 / Accepted: 3 August 1998

Abstract. The microscopic car-following model by Bando *et al.* [1–4] is extended by incorporating multi-vehicle interactions. It is shown that the reaction to more than one vehicle ahead leads to a stabilization of the dynamical behavior, *i.e.* the stable region increases. Still the fundamental macroscopic properties of traffic, free flow and congested flow, are described. More important, due to the multi-anticipative driving behavior driving in narrow platoons is forced such that a third fundamental property of traffic flow, the so-called synchronized flow [5], is modeled as well.

PACS. 64.60.Fr Equilibrium properties near critical points, critical exponents – 05.70.Fh Phase transitions: general aspects – 47.20.Ky Nonlinearity (including bifurcation theory)

1 Introduction

Over the last years scientists have shown a growing interest in traffic theory and contributions to the understanding of these complex phenomena are mainly put forward along three different lines. The macroscopic approach treats vehicular traffic as a fluid and Witham [6] was one of the first who proposed a simple hydrodynamic model. Meanwhile several higher order models are advocated [7,8]. A second, kinetic approach has been initiated by Prigogine and Herman [9]. This mesoscopic approach has recently been resumed [10,11] and has led to important improvements and a thorough understanding of hydrodynamic modeling. The third microscopic branch separates in cellular automata models [12–14] and car-following models [1,15,16]. Here every vehicle is treated individually, and due to the growing computational power cellular automata models become more and more popular. In most of the models treated so far correlations between vehicles have been neglected, but from everyday experience one knows that drivers often observe two or more nearest vehicles ahead. This leads to multi-vehicle interactions with consequences on the phase separation and the fundamental diagram. The present paper serves to investigate multi-vehicle interactions in the case of a car-following model recently proposed by Bando *et al.* [1]. We show that the reaction to more than one vehicle ahead leads to a stabilization of the dynamical behavior, *i.e.* the stable region increases. Still the fundamental macroscopic properties of traffic, free flow and congested flow, are described. More important, due to the multi-anticipative driving behavior driving in platoons is forced such that a third fundamental property of traffic flow, the so-called synchronized flow [5], is modeled as well.

[a] e-mail: henning.lenz@mchp.siemens.de

In Section 2 we introduce an extended optimal velocity model. This is followed by a linear stability analysis in Section 3. In Section 4 the characteristic properties of the proposed model are numerically investigated in terms of hysteresis loops, flux-density-relations and the speed of the fronts of a congested flow, such that a deeper understanding of the stabilizing effect of the multi-vehicle interactions will be gained.

2 Multi-following model

We extend the optimal velocity model by Bando *et al.* [1] to multi-vehicle interactions in the following way.

We suppose that drivers do not only react on the dynamics of their leading vehicle but also take into consideration up to m cars ahead with a sensitivity a_j. The dynamical equations then read[1]:

$$\ddot{x}_n = \sum_{j=1}^{m} a_j \left\{ V\left(\frac{x_{n+j} - x_n}{j}\right) - \dot{x}_n \right\}, \qquad n = 1, 2, \ldots, N. \quad (1)$$

N is the total number of vehicles and x_n is the position of the nth vehicle. For $m = 1$ we recover the original optimal velocity model.

For $V(.)$ we use the same sigmuidal function as proposed by [1], namely

$$V(x) = \tanh(x - h) + \tanh(h) \text{ with } h = constant. \quad (2)$$

[1] The car-following model by Gazis *et al.* [15] has also been extended in an additive way by Bexelius [17].

Furthermore, we introduce overall sensitivity

$$a = \sum_{j=1}^{m} a_j. \tag{3}$$

The sensitivity ratios are assumed to satisfy

$$a_j/a_1 \leq 1, \quad j = 2, 3, \ldots, m, \tag{4}$$

such that the interaction with the vehicle directly ahead is weighted the most. For simplicity, we impose periodic boundary conditions, so the vehicles travel on a circuit with length L.

3 Linear stability

It is obvious that the steady state solution of equation (1) is identical to the original model ($m = 1$), namely

$$x_n^0 = bn + ct \tag{5}$$

with

$$b = L/N, \; c = V(b), \tag{6}$$

meaning that the vehicles are equally spaced with a distance b and move forward with a velocity c. Let y_n be a small deviation from the steady state position of the nth car, *i.e.*

$$x_n = x_n^0 + y_n\,, \quad |y_n| \ll 1. \tag{7}$$

Linearization of equation (1) and neglection of higher order terms in y_n yields

$$\ddot{y}_n = \sum_{j=1}^{m} a_j \left\{ f\frac{y_{n+j} - y_n}{j} - \dot{y}_n \right\}, \tag{8}$$

where f is the derivative of V with respect to its argument, *i.e.* $f = V'(b)$.

Expanding y_n in Fourier-modes

$$y_k(n,t) = \exp\{i\alpha_k n + zt\}, \tag{9}$$

$$\alpha_k = \frac{2\pi}{N}k\,, \quad k = 0, 1, 2, \ldots, N-1. \tag{10}$$

We obtain

$$z^2 + az - f\sum_{j=1}^{m} a_j \frac{e^{ji\alpha_k} - 1}{j} = 0. \tag{11}$$

After inserting in equation (11) $z = \lambda + i\omega$, we find for the real part

$$\lambda^2 - \omega^2 + a\lambda + f\sigma_c = 0 \tag{12}$$

and for the imaginary part

$$2\lambda\omega + a\omega - f\sigma_s = 0, \tag{13}$$

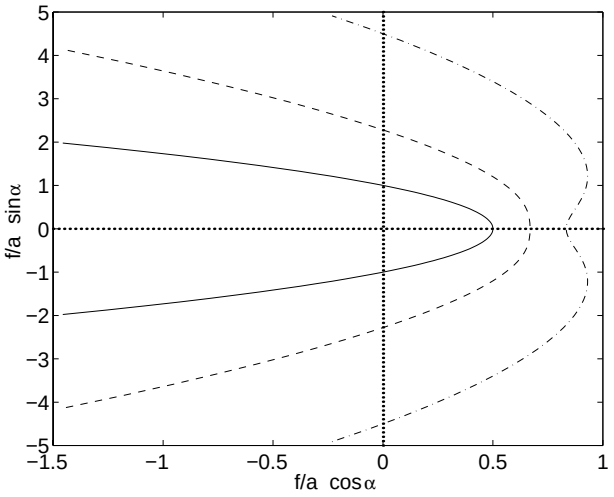

Fig. 1. The critical curves separating stable ($\lambda < 0$ – left) and unstable ($\lambda > 0$ – right) region in the $(f/a, \alpha)$ polar coordinate plane. The solid line is $m = 1$, the dashed line is $m = 2$ with sensitivity ratio $a_2/a_1 = 1/2$. The case $m = 3$ is represented by the dash-dotted line with $a_2/a_1 = 2/3$ and $a_3/a_1 = 1/3$.

where the abbreviations

$$\sigma_c = \sum_{j=1}^{m} a_j \frac{1 - \cos(\alpha_k j)}{j} \quad \text{and} \quad \sigma_s = \sum_{j=1}^{m} a_j \frac{\sin(\alpha_k j)}{j}$$

have been used. Note that $\sigma_c \geq 0$ for all α_k. Equations (12–13), together with Hurwitz's criteria then leads to the following linear stability condition ($\lambda < 0$):

$$f < \frac{a^2\sigma_c}{(\sigma_s)^2}\,. \tag{14}$$

Case m = 1

For $m = 1$ this reduces to the condition found in [1], namely:

$$f < \frac{a}{2\cos^2(\alpha_k/2)}\,. \tag{15}$$

Case m = 2

For $m = 2$ equation (14) reads

$$f < \frac{a^2\left[a_1 + a_2(1 + \cos\alpha_k)\right]\sec^2(\alpha_k/2)}{2(a_1 + a_2\cos\alpha_k)^2} \tag{16}$$

and the critical curve separating stable and unstable region is then defined by equality in equation (16). In Figure 1 the stability criteria (16) is shown in a $(f/a, \alpha)$ polar coordinate plane. The solid line depicts the case $m = 1$, whereas the case $m = 2$ with sensitivity ratio $a_2/a_1 = 0.5$ is given by the dashed line.

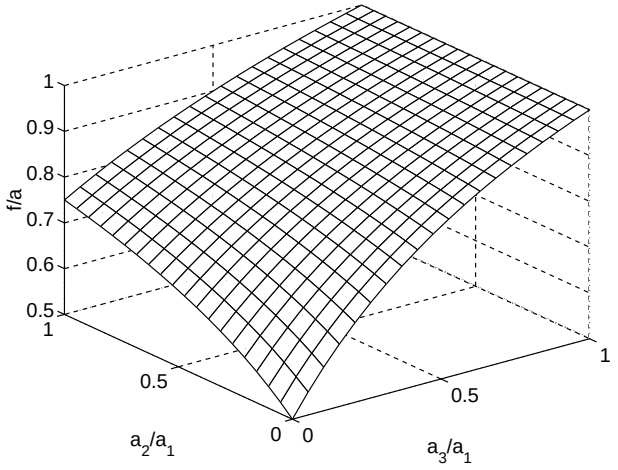

Fig. 2. f/a for the zeroth mode $\alpha_k = 0$ as a function of the sensitivity ratios a_2/a_1 and a_3/a_1.

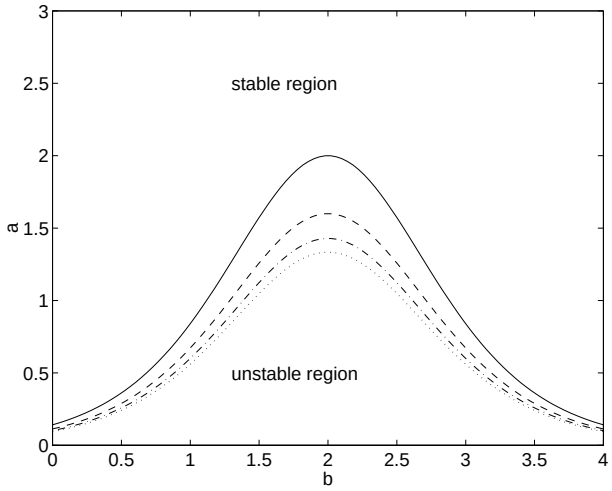

Fig. 3. Marginal stability line as function of the homogeneous spacing b for $m = 2$. The solid line corresponds to the sensitivity ratio $a_2/a_1 = 0$, the dashed line to $a_2/a_1 = 1/3$, the dash-dotted line to $a_2/a_1 = 2/3$, and the dotted line to $a_2/a_1 = 1$.

Case m = 3

For $m = 3$ equation (14) reads

$$f < \frac{a^2\left[a_1(1-\cos\alpha_k) + \frac{a_2}{2}(1-\cos 2\alpha_k) + \frac{a_3}{3}(1-\cos 3\alpha_k)\right]}{\left(a_1\sin\alpha_k + \frac{a_2}{2}\sin 2\alpha_k + \frac{a_3}{3}\sin 3\alpha_k\right)^2} \tag{17}$$

The dash-dotted line in Figure 1 shows the corresponding critical curve with sensitivity ratios $a_2/a_1 = 2/3$ and $a_3/a_1 = 1/3$.

Obviously, the most unstable mode exists near the neutral mode (see Fig. 1). Thus, it is sufficient to concentrate on the limit $\alpha_k \to 0$, where equation (14) simplifies to

$$f < \frac{1}{2}\sum_{j=1}^{m} j a_j \ . \tag{18}$$

f/a is shown in Figure 2 as a_2/a_1 and a_3/a_1 vary between zero and one. From this we conclude that (i) with a growing number of interacting vehicles and (ii) with a growing sensitivity ratio a_j/a_1 the region of stability increases. In Figure 3 the increase of the region of stability is depicted for the case, when the two nearest vehicles ahead are observed and the sensitivity ratio a_2/a_1 grows from zero to one. The stable and the unstable region are separated by the marginal stability line, where the solid line corresponds to the sensitivity ratio $a_2/a_1 = 0$, the dashed line to $a_2/a_1 = 1/3$, the dash-dotted line to $a_2/a_1 = 2/3$, and the dotted line to $a_2/a_1 = 1$.

4 Numerical simulation of traffic flow

Numerical simulations allow us to investigate whether the result of the linear stability analysis, *i.e.* the stabilizing effect of multi-vehicle interactions, also holds for the nonlinear model. Therefore, and in order to achieve physically meaningful results as well as to enhance the possibility to compare the results of our numerical simulations with real traffic data, the function V is modified according to Herrmann [4] to:

$$V(x) = v_0((1+\exp(1000/(7.35x) - 10/2.1))^{-1} - 5.34\times 10^{-9}). \tag{19}$$

In the following, the nonlinear effects of the multi-vehicle interactions on the stability of traffic flow are numerically investigated in terms of hysteresis loops, flux-density-relations and the speed of the fronts of a congested flow, such that a deeper understanding of the stabilizing effect of the multi-vehicle interactions will be gained. Besides the increase of the stable region, the multi-anticipative driving behavior leads to the formation of platoons such that synchronized flow becomes possible. Still, the common fundamental properties of traffic flow, free flow and congested flow, are modeled.

4.1 Shrinking hysteresis

For the case $m = 1$ it is well-known that for a medium homogeneous density $\rho = 1/\Delta x$ and after initialization with a small disturbance the almost homogeneous flow develops into a congested flow [1–3]. Hence, after initialization with a small disturbance the proposed model (Eq. (1)) leads for $m = 1$, $N = 300$, $L = 10$ km and $a = 0.9$ /s to a congested flow. In the Δx-$\dot{x}$-plane the profile of the congested flow is given by a hysteresis-loop as shown in Figure 4. Numerical simulation reveals that for $m = 2$, when the overall sensitivity a (Eq. (3)) stays constant, the size of the hysteresis loop shrinks simultaneously with an increasing sensitivity ratio a_j/a_1. Similarly, the size of the hysteresis loop shrinks with a growing number m of interacting vehicles. In Figure 4 the hysteresis loops are shown for the sensitivity ratios $a_2/a_1 = 0$ (or equivalently $m = 1$), $a_2/a_1 = 1/3$, $a_2/a_1 = 2/3$ and $a_2/a_1 = 1$, where the order goes from the outside to the inside.

Table 1. Characteristic properties for $m = 1$, $m = 2$ ($a_2/a_1 = 1/2$), and $m = 3$ ($a_2/a_1 = 1/2$, $a_3/a_1 = 1/4$).

m	ρ_{cr} [cars/km]	q [cars/h]	v [km/h]	$\Delta\rho_{cr}$ [%]	Δq [%]	Δv [%]	v_g [km/h]
1	19.0	1722	90.63	0.0	0.0	−0.0	−11.1
2	21.8	1885	86.50	14.74	9.47	−4.56	−23.6
3	23.6	1963	83.18	24.21	14.0	−8.2	−32.7

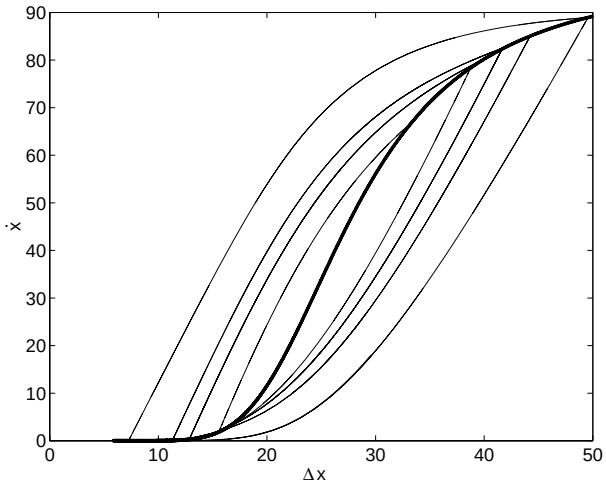

Fig. 4. Hysteresis loops of the congested flow in the Δx-$\dot{x}$-plane for $m = 2$. While the sensitivity ratio grows from $a_2/a_1 = 0$ to $a_2/a_1 = 1/3$, $a_2/a_1 = 2/3$ and $a_2/a_1 = 1$, the order goes from the outside to the inside.

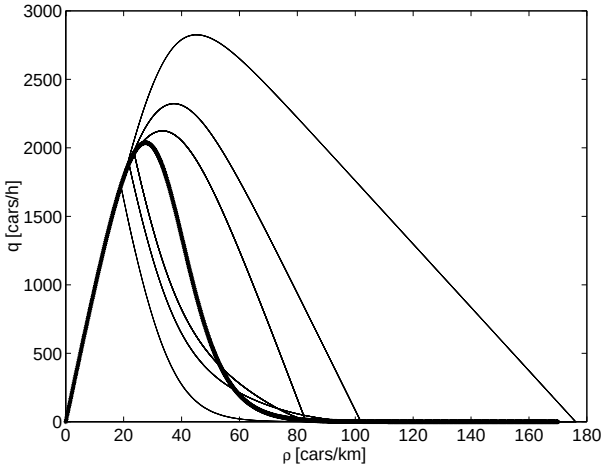

Fig. 5. Flux-density-relations for the homogeneous flow (thick line) and for congested flow with $m = 1$, $m = 2$ ($a_2/a_1 = 1/2$), and $m = 3$ ($a_2/a_1 = 1/2$, $a_3/a_1 = 1/4$) (the order goes from the outside to the inside).

4.2 Flux-density-relation

Observing the flux-density-relation gives further insights about the characteristics of the multi-anticipative car-following model. Figure 5 shows that for free flow, a homogeneous flow is realized regardless of m and regardless of the sensitivity ratios a_j/a_1 (linearly increasing part of the thick line). However, since the critical value of the density ρ_{cr} grows with increasing anticipation (see Fig. 6), also the maximum flow that is stable, *e.g.* the outflow from a congested flow, increases. In Figure 5 the flux-density-relations for a congested flow with $m = 1$, $m = 2$ ($a_2/a_1 = 1/2$), and $m = 3$ ($a_2/a_1 = 1/2$, $a_3/a_1 = 1/4$) are shown. Analogously to the shrinking hysteresis, the area covered by the flux-density-relation decreases with growing anticipation. This leads to two main effects (see Tab. 1). On the one hand, the velocity of the backwards moving stop-and-go-wave v_g depends on m and the sensitivity ratios a_j/a_1, *e.g.* it decreases from $v_g = -11.1$ km/h for $m = 1$ to $v_g = -32.7$ km/h for $m = 3$, $a_2/a_1 = 1/2$, and $a_3/a_1 = 1/4$. This fact goes conform with empirical data [18]. On the other hand, the strong increase of the critical density ρ_{cr} by 24%, is connected with a small decrease of the speed by 8% and a small increase of the flux by 14%, such that driving in narrow platoons is forced. Consequently, the increase of the stable region due to an enlarged anticipation can explain a third fundamental property of traffic flow recently investigated and named

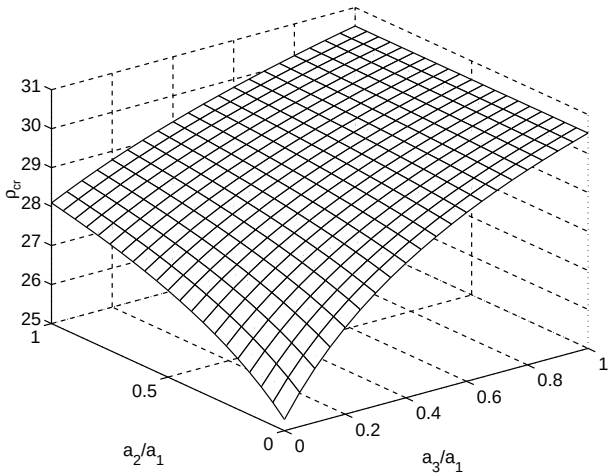

Fig. 6. Critical density ρ_{cr} for the zeroth mode $\alpha_k = 0$ as a function of the sensitivity ratios a_2/a_1 and a_3/a_1.

synchronized flow [5]. Accordingly, besides the transition from free flow to congested flow a transition from free flow to synchronized flow can exist, provided the drivers observe more than one car ahead.

5 Conclusion

In order to capture correlations between vehicles the microscopic car-following model by Bando *et al.* [1–4] has

been extended by incorporating multi-vehicle interactions. As a consequence of the multi-anticipative driving behavior, the size of the stable region increased. Besides the common fundamental properties of traffic flow, free flow and congested flow, the model was shown to reproduce a third fundamental property of traffic flow, recently investigated by Kerner and Rehborn and named synchronized flow [5]. Therefore, the model seems to be appropriate to model and predict traffic flow on highways.

References

1. M. Bando *et al.*, Phys. Rev. E **52**, 1035 (1995).
2. M. Bando *et al.*, J. Phys. I France **5**, 1389 (1995).
3. Y. Sugiyama, Workshop Traff. Dyn. Gran. Flow, 137-149 (1995).
4. M. Herrmann, B. Kerner, Physica A (submitted, 1997).
5. B.S. Kerner, H. Rehborn, Phys. Rev. Lett. **79**, 4030 (1997).
6. M.J. Lighthill, G.B. Whitham, P. R. Soc. Lond. A **229**, 317 (1955); G.B. Whitham, *Linear and nonlinear waves* (Wiley, New York, 1974).
7. B. Kerner, P. Konhäuser, Phys. Rev. E **48**, R2335 (1993).
8. P. Michalopoulos, P. Yi, A. Lyrintzis, Trans. Res. B **27**, 315 (1993).
9. I. Prigogine, R. Herman, *Kinetic Theory of Vehicular Traffic* (Elsevier, New York, 1971).
10. D. Helbing, Phys. Rev. E **53**, 2366 (1996); D. Helbing, *Verkehrsdynamik* (Springer, Berlin, 1997).
11. C. Wagner *et al.*, Phys. Rev. E **54**, 5073 (1996).
12. K. Nagel, M. Schreckenberg, J. Phys. I France **2**, 2221 (1992).
13. M. Schreckenberg, A. Schadschneider, J. Phys. A **26**, L679 (1993).
14. T. Nagatani, Phys. Rev. E **48**, 3290 (1993).
15. D. Gazis, J. Op. Res. Soc. **9**, 546 (1961); J. Phys. I France **5**, 1389 (1995).
16. A. Mason, A. Woods, Phys. Rev. E **55**, 2203 (1997).
17. S. Bexelius, Trans. Res. **2**, 13 (1968).
18. R. Sollacher, Ch. Stutz (in preparation).